Available online at www.sciencedirect.com
SCIENCE DIRECT®
International Journal of Thermal Sciences 45 (2006) 860–869
International Journal of Thermal Sciences
www.elsevier.com/locate/ijts

Dendritic counterflow heat exchanger experiments

Alexandre K. da Silva, Adrian Bejan *

Department of Mechanical Engineering and Materials Science, Duke University, Box 90300, Durham, NC 27708-300, USA

Received 5 September 2005; accepted 13 December 2005

Available online 3 February 2006

Abstract

In this paper we report experimentally the hydraulic and thermal behavior of a balanced counterflow heat exchanger in which each stream flows through a tree-shaped structure covering a circular area. The tree structure is the same on both sides of the heat exchanger: they have three channels reaching/leaving the center, and three branching levels (i.e., 24 channels on the periphery of the circular area). On the hot side, fluid is pumped from the center to the periphery. On the cold side, fluid is pumped from the periphery to the center, and leaves the heat exchanger as a single stream. Two experimental apparatuses were built and tested. In the first design, the body of the heat exchanger was made out of plexiglass and a peripheral plenum was used to collect or distribute the working fluid to the tree structure. The measurements showed that the use of a plenum generates undesirable volumetric flow asymmetries. These lessons led to a second design, which has two major improvements: (i) the heat exchanger core was made out of aluminum and (ii) individual ports (inlets/outlets) were used for each of the peripheral channels. The hydraulic results show a relation between the appearance of volumetric flow rate asymmetries and the bifurcation angles throughout the dendritic structure. The heat transfer results are also discussed.

Keywords: Constructal; Dendritic; Tree-shaped; Counterflow heat exchanger

1. Introduction

Science is marching toward smaller scales in all fields, from the Micro-Electro-Mechanical Systems (MEMS) to genome projects. Following in the same trend is the thermal engineering research, which now deals with micro- and nano-devices that dissipate increasing amounts of energy per unit area [1–19]. This means that more and more, every spacing available in a device (cooled or heated) must be used in such a way that maximal heat transfer density is achieved. There is no room for flow space that does not work for the global heat transfer enterprise.

Constructal theory and design has shown that the maximization of access can lead to high packing rates (i.e., maximal heat transfer density) if the appropriated objectives and constraints are specified [1,2]. The common feature in all the man-made constructal systems is the *natural* occurrence of a multi-scale structure, if the length scale of the device is sufficiently large, or if the smallest feature is sufficiently small. Good examples are the fluid distribution network used for cooling of electronic devices (micro- or nano-scales) to the water supply network in cities (macro-scale). This is also a common feature in fluid distribution networks of natural flow systems, which can be as wide as the Amazon River in Brazil, 1.4×10^4 m, or as small as the human bronchioles, 10^{-4} m.

A recent body of theoretical work analyzed the thermal performance of optimally designed fluid distribution networks when applied to heat transfer problems [3–7]. Bejan [3] and da Silva et al. [5] presented analytical and numerical studies of the thermal performance of dendritic heat exchangers. The results show that optimized multi-scale complexity in heat transfer devices is a promising feature.

In the present paper we describe an experimental setup built to evaluate the hydraulic and thermal behavior of a counterflow heat exchanger in which the hot and cold fluids bathe a circular area as a tree-like structure. Two experimental setups were built and tested. Both designs fall in the class of compact heat exchanges (i.e., $D_h \sim 1$ mm). The results are presented in terms of pressure drops along the dendritic structure, volumetric flow

* Corresponding author. Tel.: +1 (919) 660 5309; fax: +1 (919) 660 8963.
E-mail address: dalford@duke.edu (A. Bejan).

1290-0729/$ – see front matter © 2005 Published by Elsevier SAS.
doi:10.1016/j.ijthermalsci.2005.12.006

Nomenclature

a_i	channel width	m
A_i	channel cross-sectional area	m^2
b_i	channel depth	m
D_h	hydraulic diameter	m
f	friction factor, Eq. (3)	
g	gravity	$m\,s^{-2}$
GPH	gallons per hour	
h_w	height of water column	m
L_i	channel lenght	m
$\dot{m}$	volumetric flow rate	$m^3\,s^{-1}$
P	static pressure	Pa
R	heat exchanger radius	m
Re_{D_h}	Reynolds number, $u_{avg} D_h \rho/\mu$	
t	thickness	m
T	temperature	°C
$\Delta\overline{T}_x$	local temperature difference	°C
$u_{avg,i}$	average fluid velocity, $=\dot{m}_i/A_i$	$m\,s^{-1}$
$\dot{v}$	volumetric flow rate	$m^3\,s^{-1}$

Greek symbols

δ	uncertainty, Eq. (5)
ΔT_0	initial temperature difference between streams
λ	variables, Eq. (4)
μ	viscosity, $kg\,m^{-1}\,s^{-1}$
ρ	density, $kg\,m^{-3}$
Φ	function, Eq. (4)

Subscripts

avg	average
cold	cold stream
hot	hot stream
i	channel index
in	inlet
tot	total

rates and local temperature different between the hot and cold streams.

2. Experimental setup

The experimental prototype tested is shown in Fig. 1. The balanced counterflow heat exchanger consists of two identical trees, one for the hot fluid and other for the cold fluid. The working fluid used was tap water. The two trees mate perfectly, so that one duct of the hot tree is parallel to and in excellent thermal contact with the corresponding duct of the cold tree.

The upper part of Fig. 1 shows how the hot tree distributes the single stream of volumetric flow rate $\dot{v}_{tot}$ over the circular area occupied by the structure. The hot mini-streams are collected by a manifold on the backside of the hot tree, and are gathered as a single stream outside the heat exchanger. On the cold side, fluid is admitted into the manifold through six equidistant ports. The cold tree collects the mini-streams ($\dot{v}_i$) and forms a single cold stream ($\dot{v}_{tot}$), which is evacuated from the heat exchanger through the center of the disc.

The dendritic pattern has three pairing levels (i.e., four channel lengths, L_0, L_1, L_2 and L_3), and three L_0 channels leaving the center of the disc. This means that 24 channels are connected to the plenum on each side of the heat exchanger. The channels were machined to the same depth (1 mm) on both sides of a 3 mm-thick plexiglass disc of radius R. The thickness t that separates the hot and cold channels at every point is 1 mm.

The main dimensions of the heat exchanger are shown in Table 1. The piece of plexiglass with the channels machined into it was sandwiched between two disc-shaped lids. The lids have the same diameter as the machined part. The upper lid has a central hole through which the hot stream enters. The lower lid has a similar orifice through which the cold stream exits. Six threaded connectors were implanted in the peripheral region of each lid to allow the fluid into or out of the plenum. Once all the

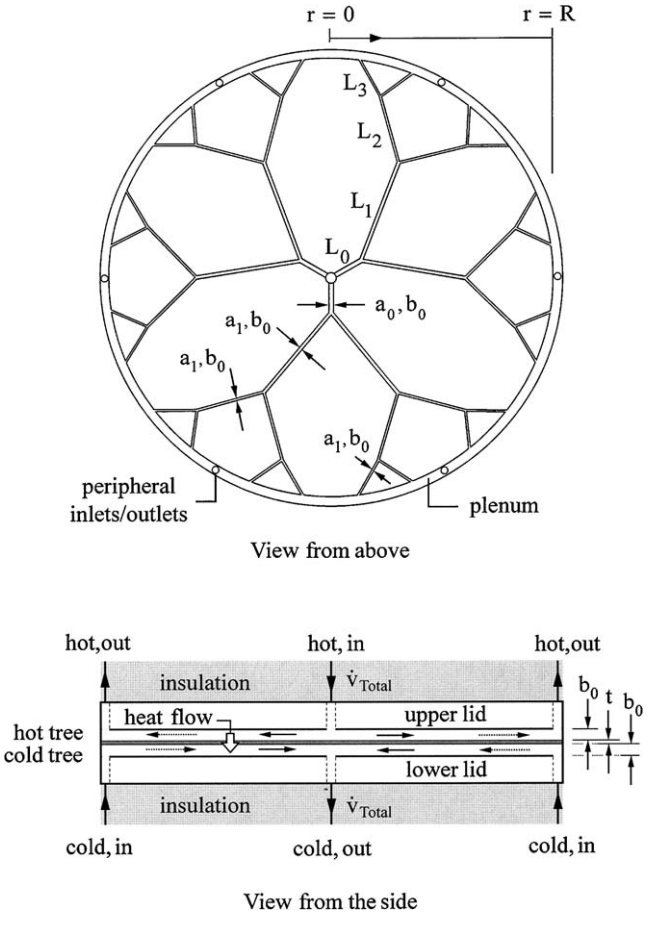

Fig. 1. Dendritic counterflow heat exchanger distributed on a disc.

taps and holes for the connectors were drilled and threaded, the three parts (heat exchanger and two lids) were glued together with a special plexiglass welder.

The flow through each side of the heat exchanger was driven by two independent constant-temperature circulators as shown

in Fig. 2. For the hot tree, the fluid was pumped from the heating circulator to a high precision control valve and then to a volumetric flow meter, before reaching the center of the hot side of the heat exchanger. After flowing through the heat exchanger, the stream was collected at six ports located on the plenum of the hot side and led into three pipes before entering a pressure equalizer. The flow then leaves the pressure equalizer as a single stream ($\dot{v}_{\text{tot}}$). On the cold side, the fluid was pumped through the control valve, the volumetric flow meter, and finally through the pressure equalizer, where the single stream ($\dot{v}_{\text{tot}}$) was separated into six identical mini-streams. The mini-streams were driven into the six ports of the plenum on the cold side, and then collected as a single stream in the center of the disc, Fig. 2.

Table 1
Dimensions of the dendritic heat exchanger shown in Fig. 1

Dimension	Value [mm]
Elemental channel thickness (a_0)	2.5
Elemental channel depth (b_0)	1
Elemental channel length (L_0)	11.6
1st, 2nd and 3rd channel branching thickness (a_1)	2
1st, 2nd and 3rd channel branching depth (a_1)	1
1st channel branching length (L_1)	44.5
2nd channel branching length (L_2)	35.7
3rd channel branching length (L_3)	19.1
Heat exchanger radius (R)	100
Plexiglass thickness between streams (t)	1
Plenum width	5
Plenum depth	1
Lid thickness	3
Diameter for the temperature and pressure taps	1.5

The heat exchanger and the tubes connecting the heat exchanger to the circulators were insulated to reduce the heat leaks from the hot tree and the heat gains to the cold tree. The initial temperature difference between the hot and cold streams was set in such way as to embrace the ambient temperature of the laboratory: this choice was made in order to reduce the heat transfer between the experimental setup and the surrounding areas.

The temperature readings were obtaining by drilling 11 taps on each lid of the heat exchanger, and two additional taps (one for each side of the heat exchanger) on the tubes that drive the two streams into the heat exchanger. The position of each tap is shown in Fig. 2. Each tap had a diameter of 1.5 mm. The tap allowed us to carefully insert a thermocouple probe (model TT-K-30 Omega) on the upper part of the flowing fluid in order to measure its local temperature. In this way we avoided disturbing the fluid flow inside the channel.

The taps used to measure temperatures were also used to measure the local static pressures. For the pressure measurements, only one side of the heat exchanger was tested. In this case, all the thermocouples were removed and replaced with threaded connectors attached to vertical transparent tubes.

The selection of the location of the taps for the temperature and pressure measurements was based on the observation that the channels at the elemental level (L_0) are symmetrically distributed around the center of the disc, where each channel receives $\dot{v}_{\text{tot}}/3$. Similarly, the flow from the elemental channels to the first pairing level is also symmetrically distributed, such that each of the six channels carries $\dot{v}_{\text{tot}}/6$. However, symmetry is broken from the second to the third pairing level, where

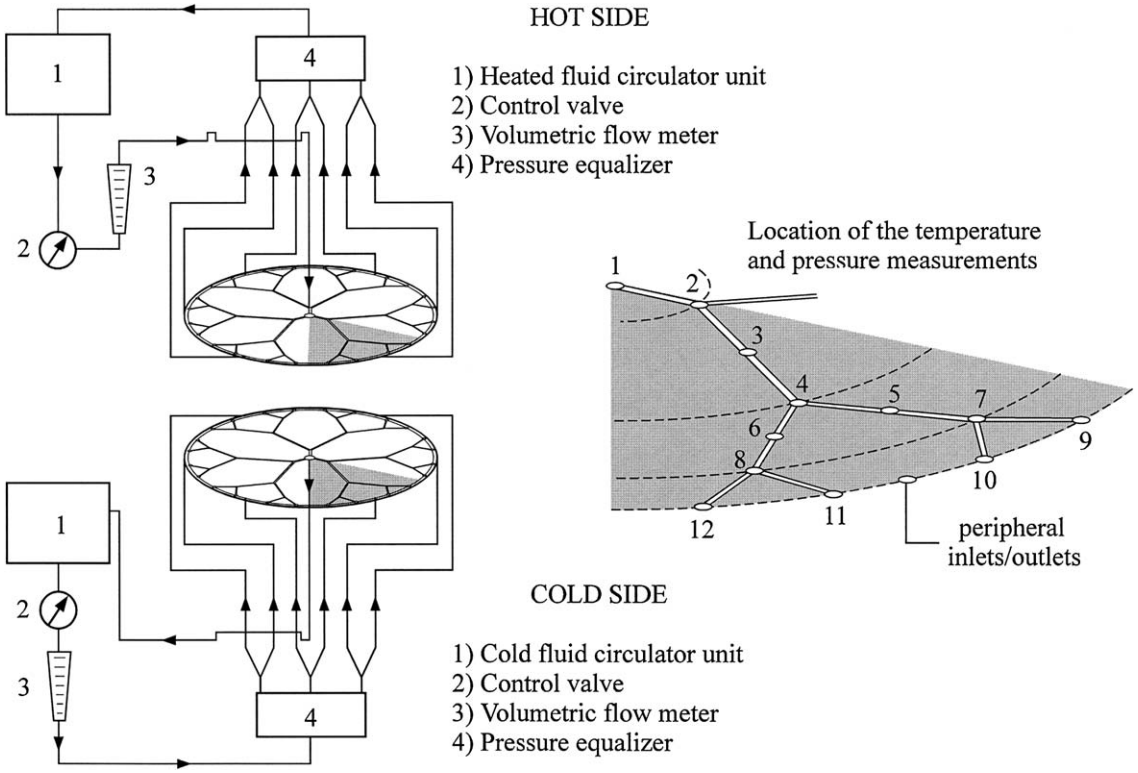

Fig. 2. Sketch of the experimental setup.

the volumetric flow rate through channel 4–8 is not necessarily the same as through channel 4–7. This asymmetric feature is transmitted from the third to the forth pairing [4].

3. Experimental procedure

All measurements were performed in steady state conditions. The pressure measurements were conducted with the fluid being pumped at 20 °C into the heat exchanger through its central port. The height of the water column was measured on one side of the heat exchanger only. The readings were taken with a vertically aligned scale, which was parallel to the transparent tubes connected to each tap. The scale precision was 1 mm. The stabilization of the water column height inside each tube was reached almost instantaneously once the total volumetric flow rate ($\dot{v}_{\mathrm{tot}}$) was set.

The stabilization toward steady state for the temperature measurements required a long and careful control of the volumetric flow rate and temperature in both fluid circulators. We made sure that the heat exchanger had no leaks, it was very well insulated, and all the thermocouples worked properly. Fluid was pumped into both sides of the heat exchanger. At the same time, two digital thermometers (Omega HH501BJK and Barnant 600–1040) monitored the inlet temperatures of the hot and cold streams. Three initial temperature difference ($\Delta T_0 = T_{\mathrm{hot,in}} - T_{\mathrm{cold,in}}$) between the hot and cold inlets were used: $\Delta T_0 = 20$, 30 and 40 °C. To avoid damage to the circulator of cooling fluid, the temperature on the cold side was set initially at $T_{\mathrm{cold,in}} = 10$ °C, and it was never lower than 9 °C.

Even though the entire system was very well insulated, heat losses or gains are inevitable, and for this reason the selected temperature for the cold fluid circulator was a little lower than 10 °C. This procedure guaranteed that the entrance temperature of the cold fluid in the heat exchanger was 10 °C even when the cold fluid gains heat on its way from the circulator to the heat exchanger. The same technique was used on the hot side, where the actual temperature selected for the fluid was a bit higher than the temperature sought for the hot stream at the entrance port. The adjustments were on the order of ±1 °C with steps of 0.1 °C. This process of checking the inlet temperatures of both streams and then adjusting the temperatures of the circulators usually took between one to two hours before the steady state was reached. This procedure was performed for each combination of ΔT_0 and $\dot{v}_{\mathrm{tot}}$ for which we ran experiments.

4. Fluid flow results

Fig. 3 shows the local static pressure measurements for five different volumetric flow rates. Pressures are expressed in terms of meters of water column ($h_{\mathrm{H_2O}}$). The values indicated in Fig. 3 can be converted to pressure units by using

$$P_{\mathrm{stc}} = h_w \rho g \tag{1}$$

where the density and gravity are, respectively, $\rho = 998.2\ \mathrm{kg\,m^{-3}}$ for water at 20 °C and $g = 9.81\ \mathrm{m\,s^{-2}}$. An interesting aspect of Fig. 3 is the effect of the total volumetric flow rate ($\dot{v}_{\mathrm{tot}}$) on the pressure drop between the four instrumented

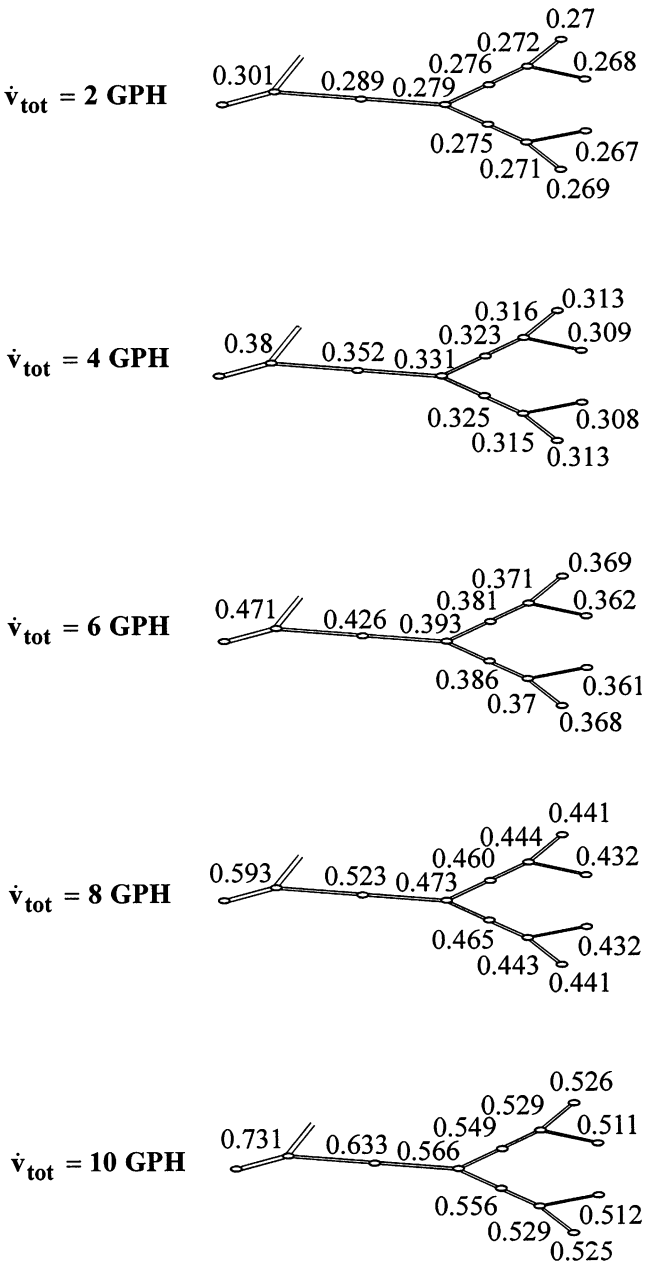

Fig. 3. Local static pressure for different mass flow rates. The number on each duct indicates the height of the water column.

channels that reach the plenum. As $\dot{v}_{\mathrm{tot}}$ increases from 2 to 10 GPH the difference between the pressure drop of the channels far from the outlet (channels 7–9 and 8–12) and the channels around the outlet (channels 7–10 and 8–11) increases. This means that most of the flow is guided toward each outlet by the channels that surround that outlet. In other words, the flow rate asymmetry between the channels of the third pairing level increases with $\dot{v}_{\mathrm{tot}}$.

From the difference in pressure between the inlet "a" and the outlet "b" of each channel, it is possible to estimate its volumetric flow rate if the flow is assumed fully developed, where

$$\dot{v}_{ab} = \frac{\pi \Delta P_{ab} D_h^4}{128 \mu L_{ab}} \tag{2}$$

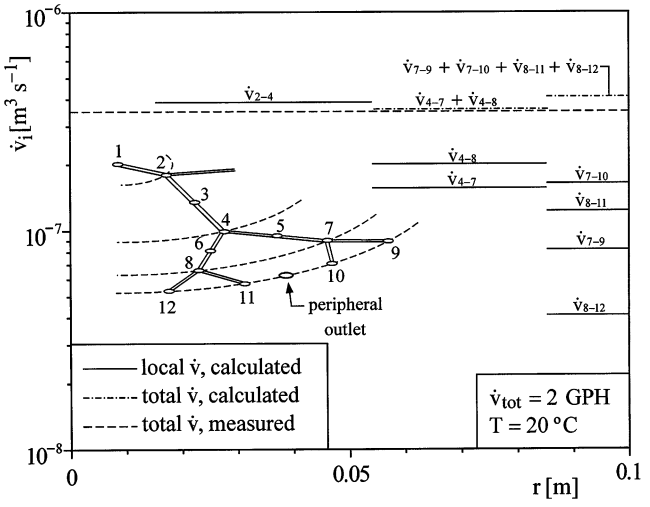

Fig. 4. Comparison of the calculated and measured volumetric flow rates.

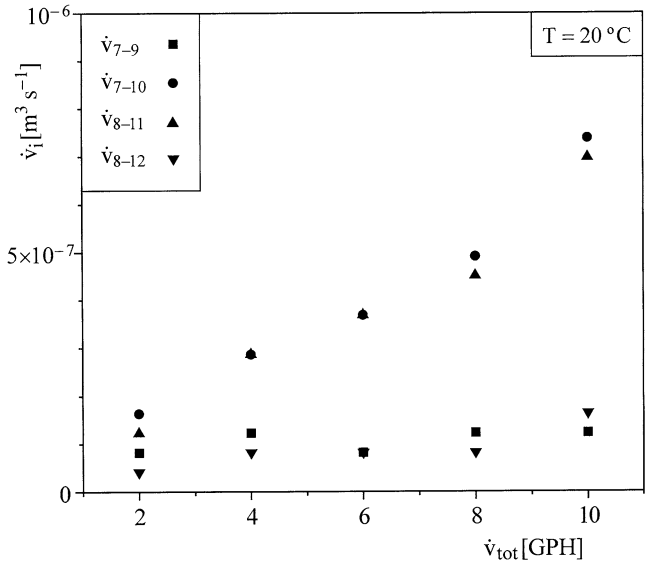

Fig. 5. Effect of the total volumetric flow rate on the volumetric flow rate of the third pairing.

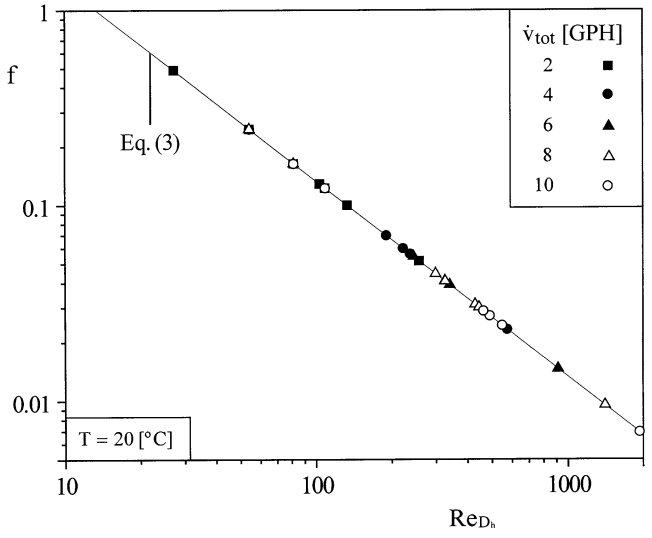

Fig. 6. Friction factor versus Reynolds number for five different total volumetric flow rates.

Fig. 4 shows the calculated volumetric flow rates (solid lines) for each channel of the first, second and third pairing levels versus the radial position of the channel. Interesting is that the volumetric flow rates through channels 7–10 and 8–11 are larger than the volumetric flow rates between through channels 7–9 and 8–12, even though inertia tends to push the fluid towards channels 7–9 and 8–12. The flow imbalance is due to the location of the outlet, which collects the fluid from the plenum. The outlet is placed symmetrically between points 10 and 11.

Fig. 4 also compares the theoretical results with the experimental measurements. Assuming that the flow arriving in the center of the heat exchanger is divided equally among the three central channels, and that the flow splitting from the central channel to the first pairing level is symmetric, one can say that the volumetric flow rate between points 2 and 4 is $\dot{v}_{2-4} = \dot{v}_{\text{tot}}/6$. A comparison with the experimental values shows a maximum deviation of 10 percent from this calculation. The volumetric flow rates through the central channels that reach the center of the heat exchanger were not calculated because the pressure at tap 1 is unknown.

Fig. 5 shows the effect of the total flow rate on the flow rate through the channels that reach the plenum. The flow rates through channels between 7–9 and 8–12 are not affected significantly by changes in the total flow rate. This behavior is compensated by a fast increase in the flow rate through channels 7–10 and 8–11 when $\dot{v}_{\text{tot}}$ increases.

Fig. 6 reports the estimated fiction factor f versus the Reynolds number (Re_{D_h}) for each channel of the structure where the pressure is known in the inlet and outlet: 2–4, 4–7, 4–8, 7–9, 7–10, 8–11 and 8–12, and for five different total flow rates. The Reynolds number (Re_{D_h}) is calculated based on the hydraulic diameter $D_h = (2a_i b_i)/(a_i + b_i)$ and on the average fluid velocity inside each channel of the exchanger $u_{\text{avg},i} = \dot{v}_i/A_i$. The fiction factor is defined as [2]

$$f = \frac{(a_i^2 + b_i^2)}{(a_i + b_i)^2} \frac{24}{Re_{D_h}} \tag{3}$$

The solid line in Fig. 6 shows that the flow is laminar in the entire range of total mass flow rate, $2 \leqslant \dot{v}_{\text{tot}} \leqslant 10$.

5. Heat transfer results

Fig. 7 shows the local temperature difference between the cold and hot streams for three different initial ΔT between the hot and cold streams, $\Delta T_0 = 10$, 20 and 30 °C. We see that as the total volumetric flow rate increases the local temperature difference between both streams also increases. This means that the flow does not reside long enough inside the heat exchanger. Another interesting observation is the asymmetric temperature difference between the two instrumented channels at the second branching level.

These results do not agree entirely with the analysis reported by da Silva et al. [5], who showed that in the counterflow formed by two balanced dendritic structures the longitudinal temperature gradient is greater closer to the canopy (plenum). Instead, the experimental results of Fig. 7 show that the tem-

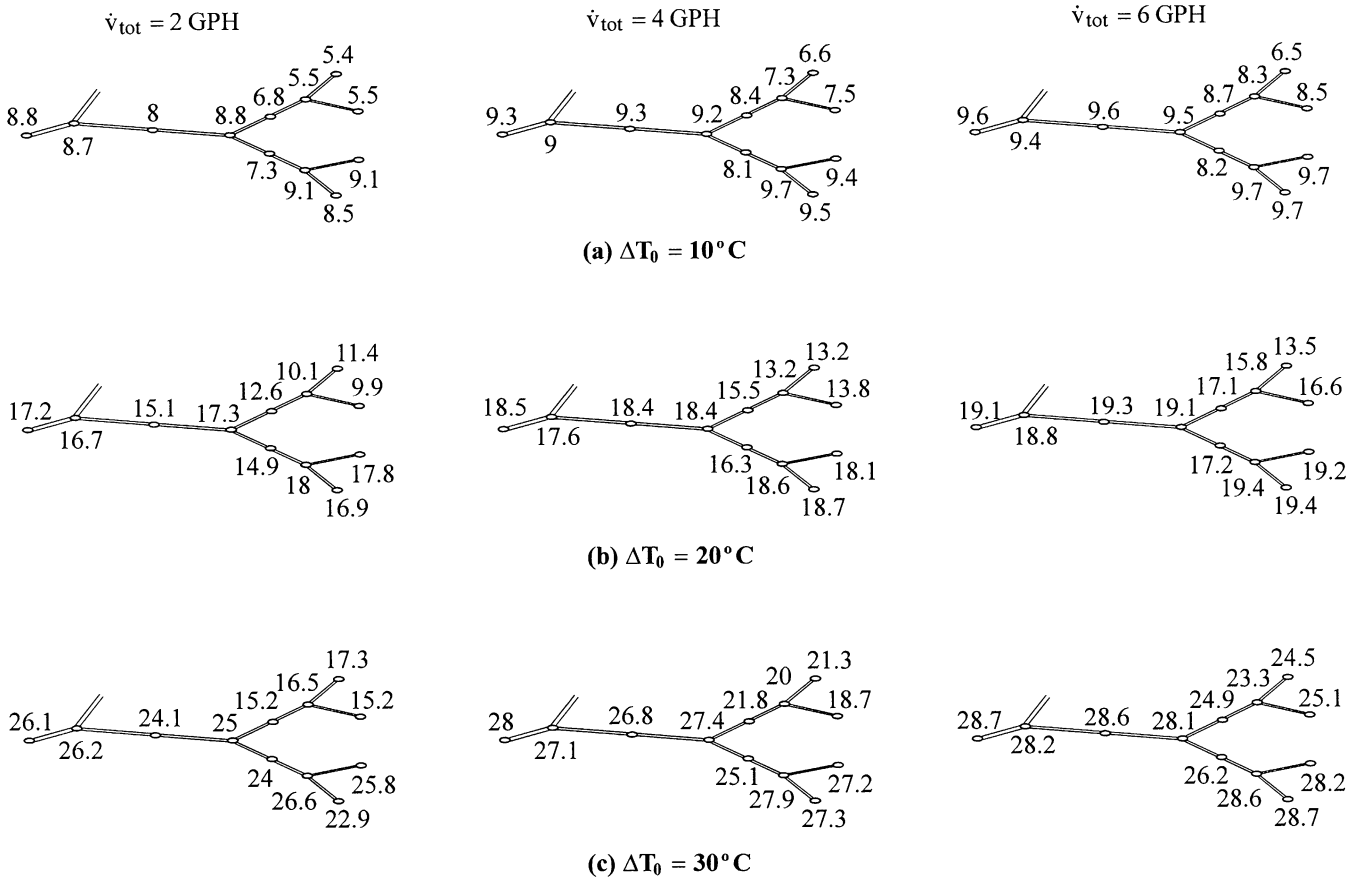

Fig. 7. Local temperature differences between the hot and cold streams.

perature differences between the hot and the cold streams (ΔT) fluctuates from the center to the periphery, with some asymmetric behavior between the two instrumented channels at the second and third branching levels.

Possible reasons for this behavior are the heat transfer design limitations of the apparatus, since the thermal conductivity of the plexiglass is very low. Also important are the locations of inlets/outlets in the plenum, which force the fluid in and out of the plenum mainly through channels 7–10 and 8–11.

6. Improved heat exchanger design

Based on the lessons learned from the first design, a new prototype is proposed in Fig. 8. The new dendritic heat exchanger presents the same number of branching levels as the one shown in Fig. 1. However, modifications have been made to improve the thermal and fluid flow of the heat exchanger.

The new design occupies only one third of the area of the original design. We made this choice by assuming that the total volumetric flow rate is divided equally among the three channels that leave the center of the heat exchanger. However, the beneficial aspect of the design is that the number of inlet/outlet ports was reduced from 24 to only 8, and now each of the eight peripheral channels located in both sides of the heat exchanger will have an individual port that connects that channel with the main stream on the outside. This feature will prevent or at least

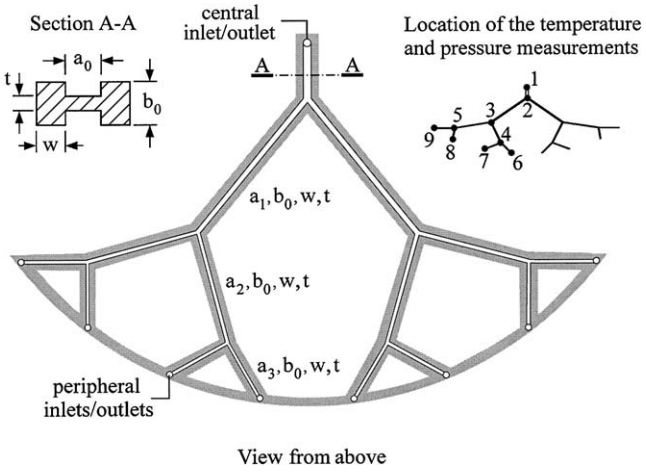

Fig. 8. Improved dendritic counterflow heat exchanger design.

minimize the asymmetry of the flow rate of channels at the third branching level.

The thermal design of the system of Fig. 8 is superior because the base material is aluminum, which has a thermal conductivity much higher than plexiglass. In addition, a thin aluminum wall surrounds each channel. The material in-between two consecutive channels has been machined out. This new construction is designed to reduce the heat loss/gain from the heat exchanger to the environment, and also the radial conductive effect throughout the body of the heat exchanger.

The new aluminum heat exchanger was also sandwiched between two plexiglass lids with the same shape and dimensions of the heat exchanger. The lids used for the new heat exchanger were much thicker (8 mm) when compared with the ones used for the first prototype (3 mm). Such simple improvement allowed us to access the heat exchanger at any time for maintenance or adjustment, because the seal between the lids and the exchanger was done by a thin layer of dried silicon, which was squashed between the aluminum and the plexiglass once the lids were bolted together. This technique provided not only a perfect hydraulic seal, but also good thermal insulation due to the low conductivity of the plexiglass. It is important to note that the bolts used to hold the three pieces together (heat exchanger and the two lids) did not touch the heat exchanger itself; they touched only the lids (i.e., the holes were drilled in the regions between two channels, where the aluminum was machined out). The main dimensions of the heat exchanger of Fig. 8 are shown in Table 2.

Fig. 9 shows the effect of the total volumetric flow rate on the mean pressure drop along the six channels of the second and third pairing levels. The bars represent the standard error (i.e., standard deviation divided by the square root of the sample size). The selection of these channels relies on the branching asymmetry outlined previously at the end of Section 2. It is important to note that the pressure drop along channels $\overline{34}$ and $\overline{35}$ is higher than the pressure drop along the peripheral channels. This happens because these two sequences of channels have the same cross-section area, which means that the fluid decelerates as it enters the channels of the third branching level. As the volumetric flow rate increases the pressure drop also increases on the peripheral channels. Also interesting is that the volumetric flow rate starts to become different in the channels of the second pairing level as $\dot{v}_{\text{tot}}$ increases (i.e., $\dot{v}_{\overline{34}} < \dot{v}_{\overline{35}}$). One possible explanation for such asymmetric behavior is the difference between the angles that connect the first and second pairing levels (i.e., $\forall_{\overline{23}\text{ and }\overline{34}} < \forall_{\overline{23}\text{ and }\overline{35}}$). This is an important finding that suggests that trees with fast flow are not necessarily symmetric (e.g. human lungs). Symmetric trees are ideal for slow flows (e.g., the flow in leaves for example). It is also worth mentioning that as the fluid flows from the 2nd to the 3rd pairing levels, the volumetric flow rate per channel decreases, and even though $\forall_{\overline{35}\text{ and }\overline{59}} < \forall_{\overline{35}\text{ and }\overline{58}}$, the volumetric mass flow rate asymmetry is not observed ($\dot{v}_{\overline{59}} < \dot{v}_{\overline{58}}$). The same can be observed for channels $\overline{34}$, $\overline{46}$ and $\overline{47}$.

In the upper frame of Fig. 10 we report the variation of the estimated friction factor f versus the Reynolds number. The friction factor f was estimated based on Eq. (3), and the Re_{D_h} was calculated based on $u_{\text{avg}} = \dot{v}/A$. Because the experimental volumetric mass flow rate in each channel is unknown, $\dot{v}$ was estimated based on Eq. (2) by assuming that the flow is fully developed. The main objective of this figure is to show that the fluid flow is mainly laminar throughout all six channels instrumented, which supports the fact that asymmetric behavior might happen in bifurcation with laminar flow. The lower frame of Fig. 10 shows the pressure drop [Pa] along the channels of

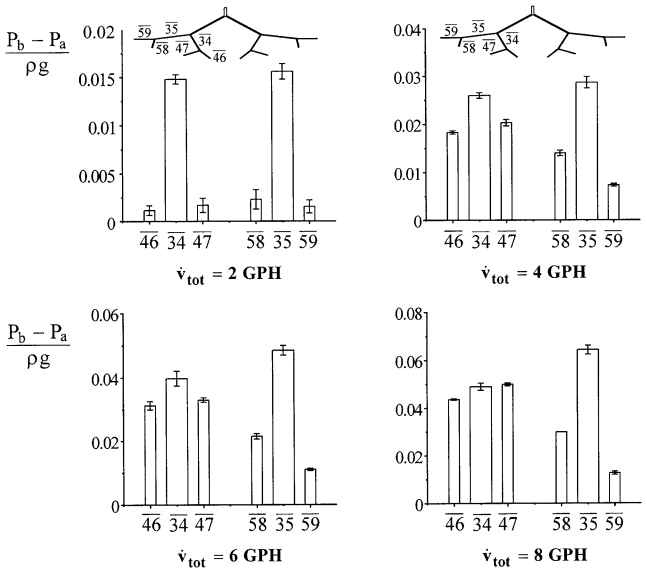

Fig. 9. Experimental values for the pressure drops along the channels of the 2nd and 3rd branching levels for $\dot{v} = 2$, 4, 6 and 8 [GPH].

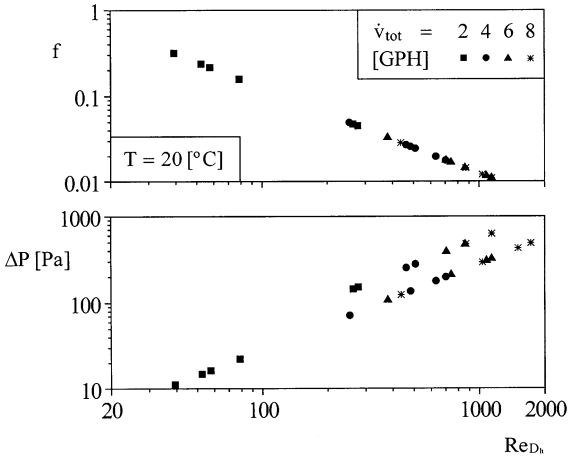

Fig. 10. Effect of the estimated Reynolds number on the friction factor (upper frame) and pressure drop (lower frame) for the channels of the 2nd and 3rd branching levels.

Table 2
Dimensions of the heat exchanger of Fig. 8

Dimension	Value [mm]
Elemental channel thickness (a_0)	2.5
Elemental channel depth (b_0)	1
Elemental channel length (L_0)	11.6
1st channel branching thickness (a_1)	2
1st channel branching depth (b_0)	1
1st channel branching length (L_1)	44.5
2nd channel branching thickness (a_2)	1.5
2nd channel branching depth (b_0)	1
2nd channel branching length (L_2)	35.7
3rd channel branching thickness (a_3)	1.5
3rd channel branching depth (b_0)	1
3rd channel branching length (L_3)	19.1
Sector radius	100
Aluminum thickness between streams	1
Lid thickness	8
Diameter for the temperature and pressure taps	1

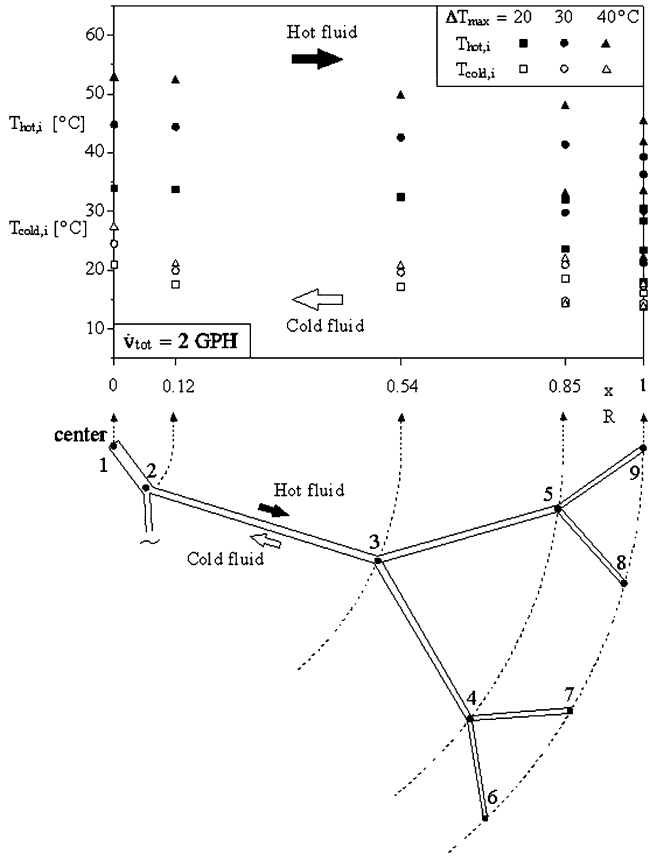

Fig. 11. Local temperature variation of the hot and cold streams along the tree structure.

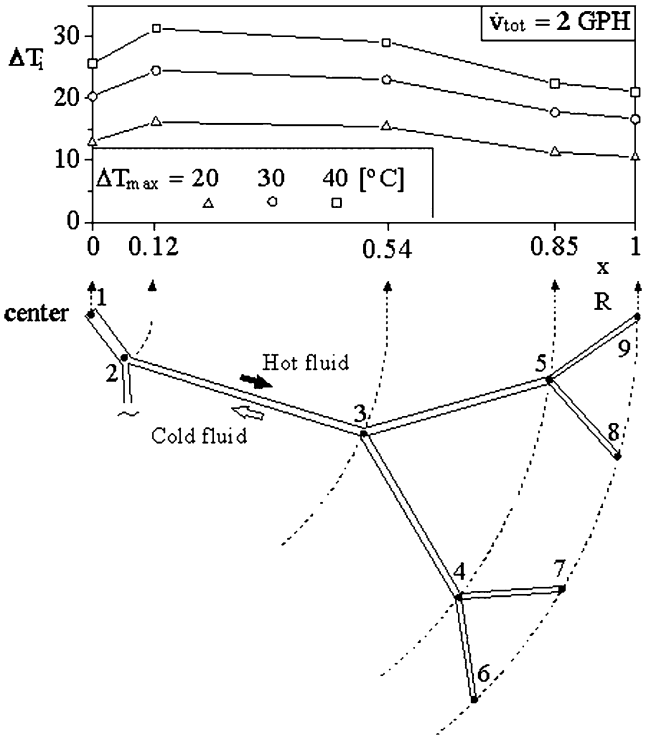

Fig. 12. Averaged temperature difference between the hot and cold streams along the tree structure.

the second and third pairing levels versus the Reynolds number. The data coalesce into two separate groups (curves): the upper group gathers the data for the channels of the 2nd pairing level, and the second group represents the data for the 3rd pairing level. These two curves converge into a single curve of constant slope if the channel length divides the pressure drop $(\Delta P_i/L_i)$.

Fig. 11 shows the temperatures of the heat and cold fluids for each one of the 9 locations where the thermocouples were installed on each side of the heat exchanger (see upper right corner of Fig. 8). The volumetric flow rate as fixed ($\dot{v}_{\text{tot}} = 2$ GPH), and $\Delta T_{\max} = (T_{\text{hot,in}} - T_{\text{cold,in}})$ was set equal to 20, 30 and 40 °C. The local temperatures were plotted against the radial location of the thermocouple on the tree structure. The lower frame of Fig. 11 shows the half-section of the experimental apparatus, which was instrumented. The dashed lines connect the thermocouple radial location (upper frame) with its physical location (lower frame). The two horizontal arrows located inside the upper frame of Fig. 11 indicate the flow direction of the hot and cold streams. Unlike in the theoretical predictions obtained by da Silva et al. [5], the temperatures of the hot and cold streams present discrepancies within the same branching level. Consider, for example, the temperature variation of the hot fluid that enters the heat exchanger with a $\Delta T_{\max} = 40$ °C, at the periphery of the heat exchanger, $x/R = 1$. Note that the solid triangles are not superimposed, instead, they are spread out. This means that the temperature of the fluid at locations 6, 7, 8 and 9 (see lower frame Fig. 11) varies. The main reason for this discrepancy relies on the fact that in Ref. [5] the heat exchanger had the same heat capacity $(\dot{v}c_p)$ in all channels of all branching levels. However, as shown in Fig. 9, the flow throughout the dendritic tree is highly asymmetric. Additionally, there is no guarantee that the streams in the hot and cold sides are identically asymmetric.

Fig. 12 shows the average temperature difference between the hot and cold streams, $\Delta\overline{T}_x = (T_{\text{hot},x} - T_{\text{cold},x})$, where the averages were calculated based on all temperature measurements for a given radial position. For example, the temperature difference between the hot and cold streams at the periphery of the heat exchanger is $\Delta\overline{T}_{x-1} = [(T_6 + T_7 + T_8 + T_9)/4]_{\text{hot}} - [(T_6 + T_7 + T_8 + T_6)/4]_{\text{cold}}$. According to Fig. 12, ΔT_x is not constant throughout the tree structure as shown by da Silva et al. [5]; instead, ΔT_x decreases toward the canopy. This is a consequence of the flow asymmetries throughout the hot and cold trees.

7. Experimental uncertainty

The experimental measurements were used to calculate the key parameters (e.g. Re_{D_h}, $\dot{v}$, f, etc.) for each instrumented channel of the heat exchanger. The uncertainty in the calculated parameters was based on the individual uncertainties of the measured quantities [20]. For example, let Φ be the calculated result, which is a given function of n independent variables:

$$\Phi = \Phi(\lambda_1, \lambda_2, \ldots, \lambda_n) \tag{4}$$

Let $\delta\Phi$ be the uncertainty in Φ, and $\delta\lambda_1, \delta\lambda_2, \ldots, \delta\lambda_n$ be the uncertainty in each independent variable. If the uncertainty

in the independent variables are given the same odds, then the uncertainty in Φ is

$$\delta\Phi = \left[\left(\frac{\partial\Phi}{\partial\lambda_1}\delta\lambda_1\right)^2 + \left(\frac{\partial\Phi}{\partial\lambda_2}\delta\lambda_2\right)^2 + \cdots + \left(\frac{\partial\Phi}{\partial\lambda_n}\delta\lambda_n\right)^2\right]^{1/2} \quad (5)$$

Consider the experimental uncertainty of the friction factor f defined in Eq. (3). In view of Eq. (4), $\Phi = f$, and the independent variables are (a_i, b_i, Re_{D_h}). If the partial derivative of f is taken with respect to the three independent variables, and then multiplied by the uncertainties of each variable, then

$$\delta f = \left[\left(\frac{\partial f}{\partial a_i}\delta a_i\right)^2 + \left(\frac{\partial f}{\partial b_i}\delta b_i\right)^2 + \left(\frac{\partial f}{\partial Re_{D_h}}\delta Re_{D_h}\right)^2\right]^{1/2} \quad (6)$$

After some algebra, Eq. (6) can be written as

$$\frac{\delta f}{f} = \left[\left(2\frac{\delta a_i}{a_i}\frac{1}{\frac{b_i^2}{a_i^2}+1} - 2\frac{\delta a_i}{a_i}\frac{1}{\frac{b_i}{a_i}+1}\right)^2 + \left(2\frac{\delta b_i}{b_i}\frac{1}{\frac{a_i^2}{b_i^2}+1} - 2\frac{\delta b_i}{b_i}\frac{1}{\frac{a_i}{b_i}+1}\right)^2 + \frac{\delta Re_{D_h}}{Re_{D_h}}\right]^{1/2} \quad (7)$$

Table 3 shows the uncertainties for the primary parameters. The uncertainty indicated for each parameter represents the maximum uncertainty found for any measurements for any channel. As for the calculated variables ($\dot{v}_i$, Re and f), the uncertainties were determined individually for each channel.

Table 4 shows the uncertainty in the local volumetric flow rate calculated based on D_h, Δh and L. The uncertainty of the volumetric flow rate between points "a" and "b" is higher for channels that reach the plenum (i.e. third pairing level). The reason is that the pressure drop in these channels is very small, and this makes it difficult to evaluate Δh. This is especially true for channels 7–9 and 8–12, in which the volumetric flow rate is insensitive to $\dot{v}_{\text{tot}}$. However, Fig. 4 showed that the local volumetric flow rates ($\dot{v}_i$) of channels 7–10 and 8–11 increase with $\dot{v}_{\text{tot}}$, which improves the experimental accuracy for these channels to the point that the uncertainty is smaller than 7% when $\dot{v}_{\text{tot}} = 10$ GPH.

Table 3
Experimental uncertainties

Parameter	Maximum error [%]
Dimensional readings (a_i, b_i, t, L_i, R, h)	±1
Local static pressure (P_i)	±1
Temperature (T_i)	±1.1
Total mass flow rate $\dot{m}_{\text{tot}}$	±4
Channel area (A_i)	±1.12
Hydraulic diameter (D_h)	±0.8

Table 4
Experimental volumetric flow rate uncertainties

$\dot{m}_{\text{tot}}$ [GPH]	1st pairing	2nd pairing		3rd pairing			
	$\dot{v}_{2-4}$	$\dot{v}_{4-7}$	$\dot{v}_{4-8}$	$\dot{v}_{7-9}$	$\dot{v}_{7-10}$	$\dot{v}_{8-11}$	$\dot{v}_{8-12}$
2	5.62	14.72	11.64	50.20	25.29	25.29	50.20
4	3.21	7.46	7.09	33.56	14.72	14.72	50.19
6	3.46	5.61	5.45	50.17	11.62	11.62	50.17
8	3.31	4.74	4.66	33.54	8.98	9.69	50.16
10	3.26	4.21	4.21	33.53	6.45	6.73	25.25

The uncertainties in Reynolds number (Re_{D_h}) and friction factor (f), which are directly or indirectly determined based on $\dot{v}_i$, show values similar to the ones presented in Table 4 for $\dot{v}_i$. The propagation of uncertainty for Re_{D_h} and f shows an increase smaller than 0.2% when compared with the uncertainty shown in Table 4 for $\dot{v}_i$.

8. Conclusions

In this paper we described the experimentally-determined hydraulic and thermal behavior of a balanced counterflow dendritic heat exchanger, in which tree-shaped structures cover a disc-shaped body. Two heat exchanger designs were tested: (i) plexiglass core assisted by a peripheral manifold, and (ii) aluminum core with individual peripheral inlets/outlets. In both designs, hot fluid was pumped from the center to the periphery, and cold fluid was pumped from the periphery to the center. The fluid entered and left the heat exchanger as a single stream. Results were obtained for several values of the total volumetric flow rate ($\dot{v}_{\text{tot}}$) and $\Delta T_{\max} = (T_{\text{hot,in}} - T_{\text{cold,in}})$.

The experimental results for the first design (Fig. 1) showed that the use of a peripheral manifold to collect or distribute working fluid to the tree-like structure generates undesirable flow asymmetries in the channels that reach the periphery. The peripheral channels that surround one of the 6 inlets/outlets located in the manifold on each side of the heat exchanger are more likely to be used as flow paths by the incoming/outgoing fluid. Such behavior agrees with the constructal law [1], which predicts that the path of least flow resistance will be generated and used. Furthermore, the heat transfer results for the first design showed fluctuations that were attributed to the low conductivity of the plexiglass core.

For the second heat exchanger design shown in Fig. 8, the experimental hydraulic results showed that the use of individual inlets/outlets for each channel reaching the periphery does reduce flow asymmetry. However, this type of design presents a major drawback when compared with the design of Fig. 1: the design of Fig. 8 requires a much more complex fluid distribution network on the periphery, while in the design of Fig. 1 complexity is reduced because of the manifold.

Another important discovery was the effect of the total flow rate on the flow rate through asymmetric bifurcations. The experimental results showed that as the total flow rate increases, the flow rates are not divided equally through the asymmetric bifurcations. This behavior suggests the existence of new (asymmetric, optimal) dendritic patterns that are able to accommodate fast flows. The heat transfer results showed that the asymmetries in the fluid flow network promote asymmetries in the temperature field throughout the dendritic structure.

In summary, this paper showed the first construction and testing of a compact and complex dendritic structures, which were theoretically anticipated and tested in Refs. [4,5,21]. Con-

ceptually, this paper represents a step toward the next generation of heat exchangers with maximum density.

Acknowledgements

A.K. da Silva's graduate studies at Duke University were supported by the Brazilian Research Council–CNPq (Conselho Nacional de Desenvolvimento Científico e Tecnológico), Brazil. A. Bejan's research was supported by a grant from the Air Force Office of Scientific Research. The authors thank Mr. Mauro Robbe and Profs. Sylvie Lorente and Enrico Sciubba for guidance and comparisons with numerical simulations of similar tree-shaped heat exchanger architectures. The authors also thank Mr. Tony Knight and John Goodfellow II (Department of Mechanical Engineering and Materials Science, Duke University) for the numerous suggestions during the construction of the experimental prototypes.

References

[1] A. Bejan, Shape and Structure, from Engineering to Nature, Cambridge University Press, Cambridge, UK, 2000.
[2] A. Bejan, Convection Heat Transfer, third ed., Wiley, New York, 2004.
[3] A. Bejan, Dendritic constructal heat exchanger with small-scale crossflows and larger-scales counterflows, Int. J. Heat Mass Transfer 45 (2002) 4607–4620.
[4] W. Wechsatol, S. Lorente, A. Bejan, Optimal tree-shaped networks for fluid flow in a disc-shaped body, Int. J. Heat Mass Transfer 45 (2002) 4911–4924.
[5] A.K. da Silva, S. Lorente, A. Bejan, Constructal multi-scale tree-shaped heat exchanger, J. Appl. Phys. 96 (2004) 1709–1718.
[6] J. Bonjour, L.A.O. Rocha, A. Bejan, F. Meunier, Dendritic fins optimization for a coaxial two-stream heat exchanger, Int. J. Heat Mass Transfer 47 (2004) 111–124.
[7] J.C. Ordóñez, A. Bejan, Entropy generation minimization in parallel-plates counterflow heat exchangers, Int. J. Energy Res. 24 (2000) 843–864.
[8] J.E. Hesselgreaves, Compact Heat Exchangers: Selection, Design and Operation, Pergamon, Amsterdam, 2001.
[9] A.D. Kraus, A. Bar Cohen, Design and Analysis of Heat Sinks, Wiley, New York, 1995.
[10] W.M. Kays, A.L. London, Compact Heat Exchangers, third ed., McGraw-Hill, New York, 1984.
[11] J. Peterson, Y. Bayazitoglu, Optimization of cost subject to uncertainty constraints in experimental fluid-flow and heat-transfer, J. Heat Transfer 113 (1991) 314–320.
[12] G.P. Celata, M. Cumo, G. Zummo, Thermal-hydraulic characteristics of single-phase, flow in capillary pipes, Exp. Thermal Fluid Sci. 28 (2004) 87–95.
[13] B. Agostini, B. Watel, A. Bontemps, B. Thonon, Liquid flow friction factor and heat transfer coefficient in small channels: An experimental investigation, Exp. Thermal Fluid Sci. 28 (2004) 97–103.
[14] W. Owhaib, B. Palm, Experimental investigation of single-phase convective heat transfer in circular microchannels, Exp. Thermal Fluid Sci. 28 (2004) 105–110.
[15] P.S. Lee, S.V. Garimella, D. Liu, Investigation of heat transfer in rectangular microchannels, Int. J. Heat Mass Transfer 48 (2005) 1688–1704.
[16] H.B. Ma, G.P. Peterson, Laminar friction factor in microscale ducts of irregular cross section, Microscale Thermophys. Engrg. 1 (1997) 253–265.
[17] X.P. Peng, G.P. Peterson, Convective heat transfer and flow friction for water flow in microchannel structures, Int. J. Heat Mass Transfer 39 (1996) 2599–2608.
[18] W.L. Qu, I. Mudawar, Experimental and numerical study of pressure drop and heat transfer in a single-phase micro-channel heat sink, Int. J. Heat Mass Transfer 45 (2002) 2549–2565 .
[19] S.J. Kim, S.W. Lee, Air Cooling Technology for Electronic Equipment, CRC Press, Boca Raton, FL, 1995.
[20] J.P. Holman, Experimental Methods for Engineers, McGraw-Hill, New York, 1978.
[21] W. Wechsatol, S. Lorente, A. Bejan, Dendritic convection on a disc, Int. J. Heat Mass Transfer 46 (2003) 4381–4391.